

Article

Nature of Perovskite Mineralization of Silicate-Carbonate Veins in the Margins of Kusinsko-Kopanskaya Layered Intrusion (South Urals, Russia)

Sergey Stepanov¹, Roman Palamarchuk^{1,*}, Anton Kutyrev² , Elena Lepekhina³, Ludmila Sharpenok³, Evgeniy Shagalov⁴ and Elena Minervina⁵

¹ South Urals Research Center of Mineralogy and Geocology of the UB RAS, 456317 Miass, Russia; stepanov-1@yandex.ru

² School of Earth and Environmental Sciences, Cardiff University, Cardiff CF10 3AT, UK; anton.v.kutyrev@gmail.com

³ A.P. Karpinsky Russian Geological Research Institute, 199106 Saint-Petersburg, Russia

⁴ Zavaritsky Institute of Geology and Geochemistry of the UB RAS, 620010 Yekaterinburg, Russia

⁵ Institute of Geology of Ore Deposits, Petrography, Mineralogy and Geochemistry of the RAS, 119991 Moscow, Russia

* Correspondence: palamarchuk22@yandex.ru; Tel.: +7-981-9799395

Abstract: This study presents the first comprehensive investigation of perovskite from its type locality (Mineral Mines of Southern Urals, Russia), where this mineral was first described by Gustav Rose in 1839. The new data includes results from precise chemical analyses (electron-probe microanalyzer, LA-ICP-MS) and U-Pb ages (SHRIMP-II) of perovskite. Perovskite occurs in silicate-carbonate veins that transect the marginal parts of the Middle Rhiphaean Kusinsko-Kopanskaya layered intrusion, previously thought to be skarns. The perovskite crystals range from micrometer-scale grains to up to 11 cm in size. Chemical investigations revealed a low content of trace elements (rare earth elements, Y, Nd, U, Th) compared to perovskites from alkaline ultramafic rocks, silica-undersaturated basic rocks, carbonatites, and kimberlites. The determined age of the perovskite, 535 ± 43 Ma, significantly differs from the 1379 ± 8 Ma age of the Kusinsko-Kopanskaya intrusion, challenging the skarn-origin hypothesis for perovskite. Instead, the findings suggest a carbonatite origin for the perovskite mineralization. This timing indicates a previously unknown stage of endogenic activity on the Western Slope of the Southern Urals.

Keywords: perovskite; LA-ICP-MS; U-Pb dating; Southern Urals Western slope; Kusinsko-Kopanskaya layered intrusion; carbonatite; kimberlite; silica-undersaturated rocks



Citation: Stepanov, S.; Palamarchuk, R.; Kutyrev, A.; Lepekhina, E.; Sharpenok, L.; Shagalov, E.; Minervina, E. Nature of Perovskite Mineralization of Silicate-Carbonate Veins in the Margins of Kusinsko-Kopanskaya Layered Intrusion (South Urals, Russia). *Minerals* **2024**, *14*, 478. <https://doi.org/10.3390/min14050478>

Academic Editor: Jaroslav Dostal

Received: 21 March 2024

Revised: 25 April 2024

Accepted: 27 April 2024

Published: 30 April 2024



Copyright: © 2024 by the authors. Licensee MDPI, Basel, Switzerland. This article is an open access article distributed under the terms and conditions of the Creative Commons Attribution (CC BY) license (<https://creativecommons.org/licenses/by/4.0/>).

1. Introduction

1.1. Historical Background

Perovskite CaTiO_3 was initially described in 1839 by mineralogist Gustav Rose [1] in the samples from the Akhmatov mine (Southern Urals, Russia). These samples were discovered in 1811 during exploration activities aimed at locating abrasive garnet, and the mine was named in honor of the mining engineer E.F. Akhmatov. For a long time, Akhmatov mine was the only source for large handpieces of perovskite [2,3]. After the accumulation of new data on the geological structure of Southern Urals and targeted prospecting works on abrasive garnet, other mines mineralogically analogous to the Akhmatov mine were discovered. These sites (hereafter referred to as the Nazyam mountains mines) are spatially associated with the Middle-Riphaean Kusinsko-Kopanskaya layered intrusion. Diverse mineral bodies, predominantly silicate-carbonate veins, were revealed by mining activities during exploration and extraction [4]. In addition to the Akhmatov mine, perovskite-rich mines include Nikolae-Maksimilianov (discovered in 1867 and named after N.M. Leuchtenberg, the chairman of the Russian Mineralogical Society), Zelentsov (discovered in 1929

and named after engineer S.M. Zelentsov), and Perovskite. The latter two mines, which are currently more accessible, were used for this study.

1.2. Modern Studies of Perovskite

Currently, perovskite and related minerals in the perovskite group are extensively researched due to their broad distribution in alkaline-ultramafic complexes with carbonatites and kimberlites [5–10]. These studies focus on various aspects, including patterns in perovskite's chemical composition, which provide insights into the nature of perovskite mineralization. However, perovskite from its type locality in the Southern Urals has been less studied for several reasons. Notably, comprehensive data on the chemical composition of perovskites from the Akhmatov mine and adjacent mineral deposits, covering both principal components and trace elements, remains elusive.

Since its discovery, the perovskite mineralization in the Nazyam mountains has been attributed to skarns, which formed at the contact between the Kusinsko-Kopanskaya intrusion and the dolomites of the Satka formation [11]. However, emerging evidence that highlights a significant divergence between the perovskite mineralization and the rocks of the Kusinsko-Kopanskaya intrusion has led to the proposal of alternative origins, specifically metamorphic [12] and carbonatitic [13,14].

In summary, the origin of perovskite in the silicate-carbonate veins of the Akhmatov mine and other locations remains unclear. This paper employs a range of contemporary mineralogical, geochemical, and geochronological techniques to provide the first comprehensive analysis of perovskite from its primary discovery site. This investigation is expected to shed light on the origins of this mineral and significantly enhance our understanding of the endogenic processes on the Western slope of the Southern Urals.

2. Geological Setting

The studied mines are located in the Bashkirsky anticlinorium of the Central Urals uplift (Figure 1). This study focuses on silicate-carbonate veins extracted along the contact of the Kusinsko-Kopanskaya gabbro intrusion (Figure 1c). The age of this intrusion, determined by U-Pb zircon dating, is Middle Riphean, specifically 1379 ± 8 Ma [15]. The intrusion features a layered structure, consisting of alternating melanocratic and leucocratic types of gabbro. It also contains concordant layers of Ti-magnetite ore, aligned with the original magmatic stratification, extensively exploited for titanium during the 20th century. The metamorphic gradation of the Kusinsko-Kopanskaya intrusion varies, with its northern segment reaching amphibolitic facies, while the southern section exhibits only minor metamorphic changes. The contemporaneous Ryabinovsky granitic intrusion lies adjacent to these mafic structures. To the west, these complexes intrude into the limestones of the Lower Riphean Satka formation, while to the east, they contact the metabasites of the Lower Riphean Kuvash formation through a system of regional faults (Figure 1c).

The Zelentsov mine consists of silicate-carbonate veins that cut across the metamorphosed gabbro of the Kusinsko-Kopanskaya intrusion in a discordant manner. Located at the site of an abandoned Ti-magnetite mine (Figure 2), the veins are primarily composed of calcite with variable amounts of olivine and magnetite in different parts of the veins. At the eastern inner contact of the mine, there is a thick olivine pegmatite vein containing large euhedral olivine crystals (up to 20 cm in size), along with magnetite, perovskite, clinocllore, clintonite, and other minerals. These cavities are filled with coarse-grained calcite aggregate. At the western inner contact, there is a vein composed mainly of hydrotalcite-2H, with smaller amounts of clinohumite, magnetite, and spinel. The veins contain numerous cavities filled with coarse-grained calcite and hydrotalcite-2H. The walls of these cavities are lined with euhedral crystals of magnetite, perovskite, and spinel.

The metamorphosed gabbro has undergone metasomatic alteration, resulting in the formation of chlorite only or aggregates of garnet and chlorite. These aggregates contain cavities filled with coarse-grained calcite and druses of clinocllore and magnetite, including sporadic cubic perovskite and rhombohedral garnet crystals. Epidote, epidote-hornblende, and

hornblende metasomatites are prominent among the metasomatic rocks after the gabbro. The altered rocks form complex, vein-like bodies with cavities up to 0.5 m in size filled with coarse-grained calcite. Euhedral crystals of epidote and hornblende incrustate the walls of cavities.

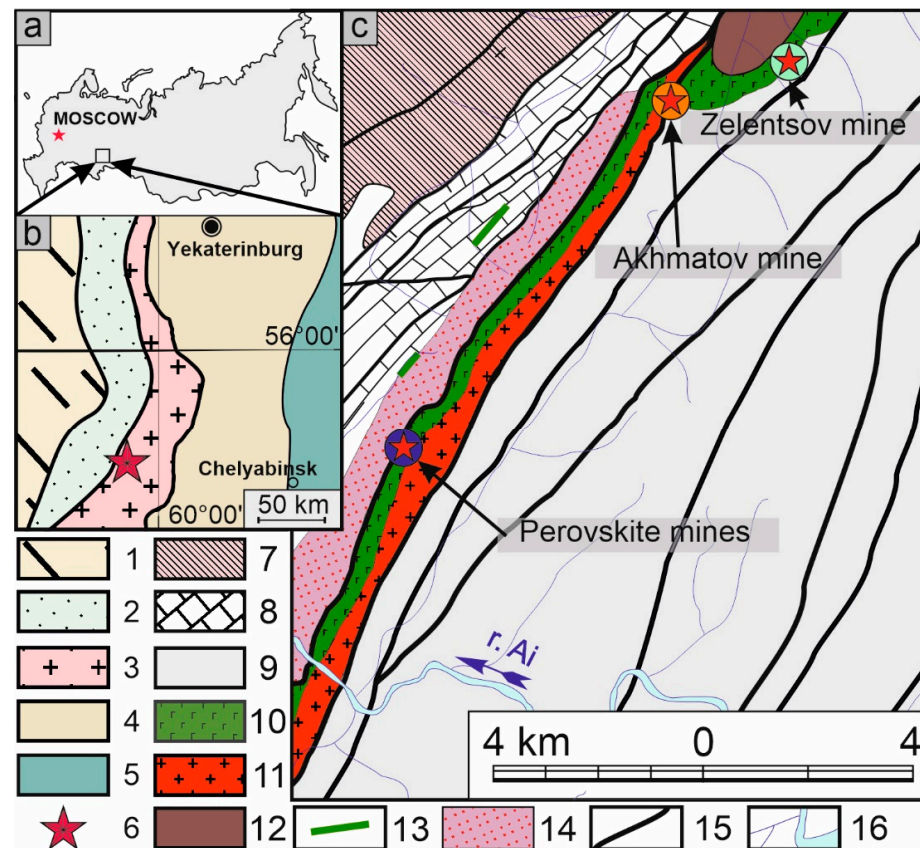


Figure 1. Geological position of Mineral Mines in the Russian map (a), in the tectonic scheme of Ural Mountains (b) and a geological sketch of the northern part of the Kusinsko-Kopanskaya layered intrusion (c): 1—Paleozoic sedimentary rocks of the East-European Platform, 2—West-Urals Fold and Thrust Zone, 3—Central Urals Uplift, 4—Tagil-Magnitogorsk Megazone, 5—Mesozoic and Cenozoic formations of West-Siberian Platform, 6—location of the Kusinsko-Kopanskaya layered intrusion in the tectonic scheme, 7—sandstones, aleurolites (siltstones), basalt flows, carboniferous shales, sandy dolomites of Low-Riphean Ai formation, 8—dolomites of Low-Riphean Satka formation, 9—metamorphic shales and amphibolites of Middle-Riphean Kuvash formation, 10—Middle-Riphean Kusinsko-Kopanskaya layered intrusion, 11—Middle-Riphean Ryabinovsky granite intrusion, 12—Devonian (?) dolomites, limestones and shales, 13—Upper-Riphean gabbro-dolerite dikes, 14—skarns and hornfels zone, 15—major faults, 16—the Ai river.

Perovskite mines are located in areas where the Kusinsko-Kopanskaya gabbro intrusion is not exposed on the surface. In these areas, mining reveals recrystallized dolomites of the Satka formation, intersected by thick, mineralized calcite bodies containing up to 5% magnetite, clinohumite, clinochlore, and other minerals in smaller quantities. These bodies host veins composed of magnesium-enriched silicaterocks of four mineral composition varieties: clinochlore-serpentine, serpentine-clinochlore, diopside-chlorite, and serpentine only (Figure 3). The veins typically measure about 0.7 m in thickness (extending up to 2.1 m in some parts), containing numerous cavities, some of which are as large as 0.4 m in diameter. These cavities are mostly filled with medium-grained calcite aggregates. It is noteworthy that walls of cavities are adorned with druses of euhedral clinochlore, magnetite, and perovskite. The size of an individual clinochlore crystal is up to 12 cm, the largest magnetite crystal is up to 24 cm, and the longest edge of the largest perovskite crystal is 7.8 cm.

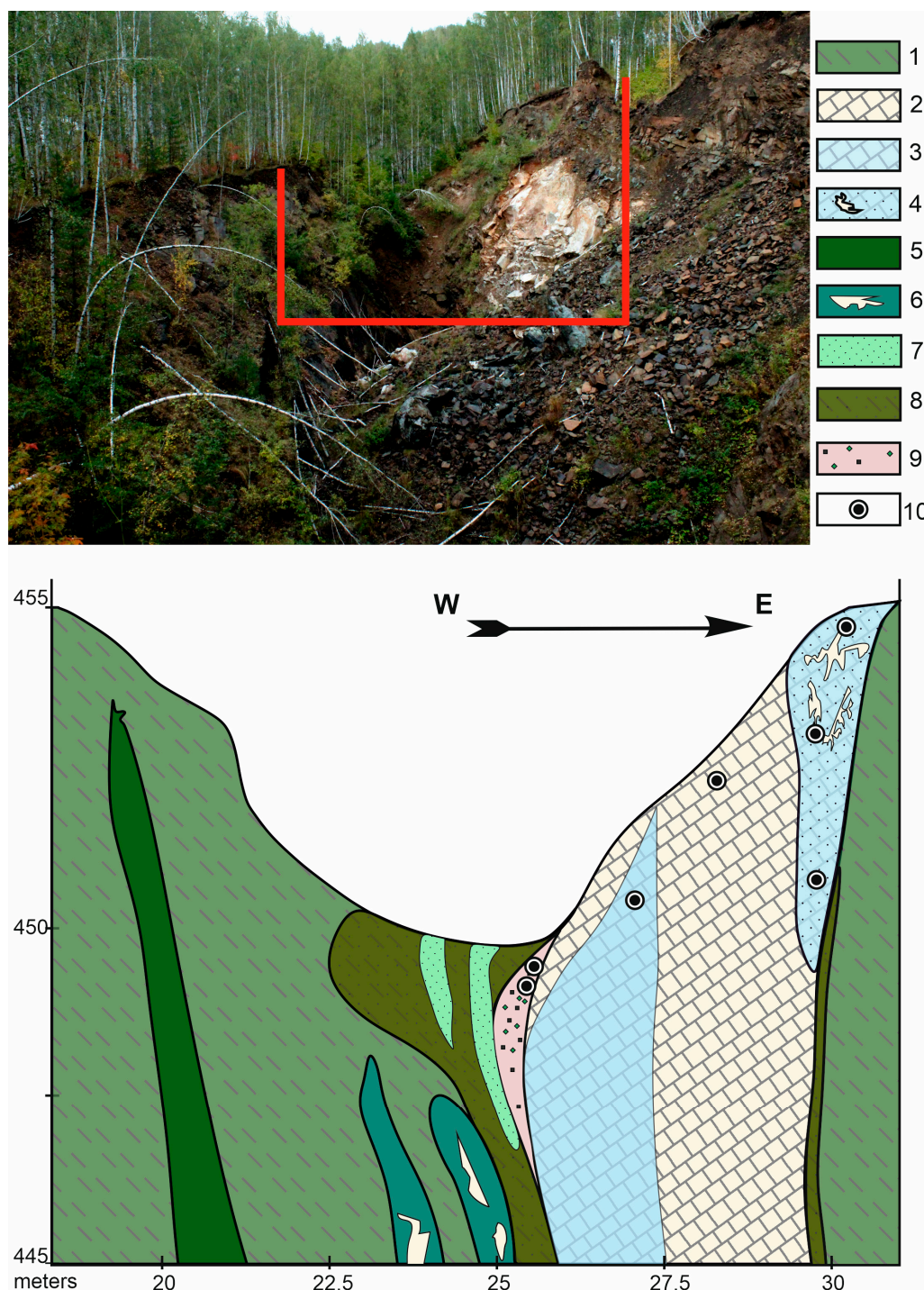


Figure 2. A photo of the failure zone in the Ti-magnetite mine of Kusinskoye deposit combined with the schematic cross-section of Zelentsov mine (cross-section projection is marked by the red line on the photo above): 1—metamorphosed gabbro and amphibolites, 2—coarse-grained calcite rocks with subordinate amount of olivine and magnetite, 3—magnetite-forsterite-calcite rocks, 4—pegmatitic forsterite rocks with cavities filled by calcite, 5—amphibole-epidote metasomatic rocks after gabbro, 6—coarse-grained amphibole-epidote rocks with mineralized calcite cavities, 7—coarse-grained clinocllore rocks with rare calcite cavities, 8—magnetite-garnet-clinocllore metasomatic rocks after gabbro, 9—clinocllore-hydrotralcite-2H rocks with cavities filled with calcite, magnetite, spinel, and perovskite, 10—sampling points.

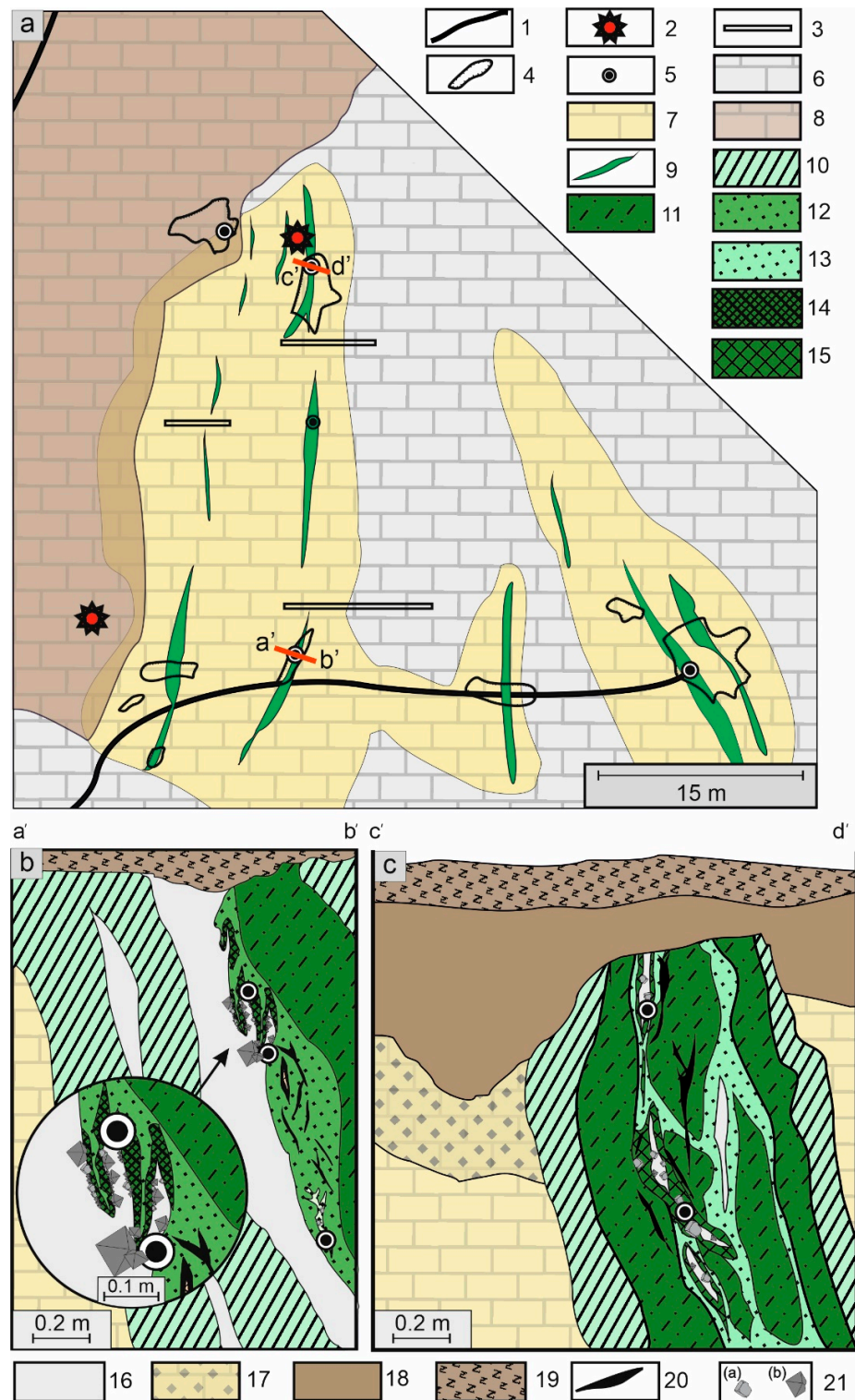


Figure 3. Geological sketch of Perovskite Mine (a) and the typical cross-sections (b,c) of silicate-carbonate veins with magnetite and/or perovskite mineralization: 1—forest roads, 2—base camp, 3—prospecting trenches, 4—excavation contours, 5—sampling points, 6—marbled limestones, 7—calcite mineralized rocks, 8—clay, 9—serpentine-chlorite, chlorite-serpentine, and diopside-chlorite veins, 10—serpentine rocks, 11—serpentine-chlorite rocks, 12—chlorite rocks, 13—ophite-chlorite rocks, 14—clinocllore-magnetite coarse-grained rocks, 15—coarse-grained chlorite rocks, 16—coarse-grained calcite rock, 17—weathered marbles, 18—deluvial clay, 19—soil, 20—magnetite veins, 21—large crystals of perovskite (a) and magnetite (b).

3. Material and Methods

3.1. Sample Collection

This study is based on fieldwork conducted by the authors from 2012 to 2019. Samples were collected from the Zelentsov and Perovskite mines, with all mines meticulously documented. The collection includes over 85 hand specimens, comprising a total of 347 individual perovskite crystals that were studied. The sizes of the crystals ranged from 0.3 cm to 8.7 cm. Perovskite crystals of different habits or occurring in different mineral parageneses were sliced to investigate their internal zonal and sectoral structures. The crystal faces of perovskite were determined using a bicircular reflecting goniometer.

3.2. Analytical Methods

Polished sections of hand specimens were investigated using optical and electron microscopy. A preliminary study of the perovskite composition and accompanying minerals was conducted using a JEOL-JSM6390LV scanning electron microscope equipped with an EDS Inca Energy 450 X-Max 80 from Oxford Instruments at the Institute of Geology and Geochemistry RAS, Yekaterinburg, within the collective use center “Geoanalytic”. Additionally, a Tescan VEGA-3 system equipped with an Oxford XMax 80 EDS detector was employed at the Institute of Volcanology and Seismology, Petropavlovsk-Kamchatsky. The precise chemical composition was determined using a Cameca SX-100 equipped with five wavelength-dispersive spectrometers. The analysis conditions were set to a 15 kV accelerating voltage and a 30 nA beam current. Standards used included Ca and Mg—diopside, Mn—rhodonite, Fe—Fe₂O₃, Ti—rutile, Al—jadeite, REE and Y—silicate glasses of the corresponding metals, U—UO₂, P—apatite, and Zr and Hf—zircon.

The content of minor elements was investigated using LA-ICP-MS. The analyzed crystals were sliced through their geometric center to evaluate their zonal structure correctly and were then mounted into a standard 1-inch sample. The experiments were carried out using the X-Series II mass spectrometer coupled with the NWR-213 sampling system. The analyses were performed using a laser beam size of 60 µm, a pulse rate of 10 Hz, and an energy of 18–19 J. Sensitivity calibration was performed using a standard 11-element solution. Standard 68-element solutions, ICP-MS-68A, HPS, and solutions A and B with concentrations of 10 and 50 µg/L, respectively, were used to calibrate the mass peaks and detectors. The intensity of the laser ablation signal was measured using silicate glass NIST SRM 612. The analytical error for different elements varied from 1–3% for REE, U, Th, and Pb, to 30–50% for Ni, Zn, Cu, and Co. Element concentrations were determined using NIST SRM 610 and 612 silicate glass standards, which closely match the matrix compositions of the samples.

After investigating the distribution of trace elements in perovskites using LA-ICP-MS, the age of the same crystals was determined by the U-Pb method. Measurement of uranium, lead, and thorium isotope concentrations in the sample crystals was carried out by the ion-mass spectrometric method (SHRIMP-II). The perovskite from the Tazheran Massif, proposed as a standard in the works of [16,17], was used as a reference material. The ²⁰⁶Pb/²³⁸U ratios were normalized to 0.074465, corresponding to an age of 463 million years [16].

4. Results

4.1. Parageneses with Perovskite

Perovskite is a common mineral found in silicate-carbonate veins in mines such as Zelentsov, Perovskite, and others located near the Kusinsko-Kopanskaya intrusion. At the Zelentsov mine, three common parageneses have been identified: (A) perovskite-magnesioferrite-forsterite-calcite (Figure 4a,b,d), (B) perovskite-garnet-clinocllore-calcite, and (C) perovskite-spinel-hydroxycalcite-2H-calcite (Figure 4c). In some rocks, perovskite can be referred to as a rock-forming mineral, comprising up to 5% of the total rock volume. These rocks contain euhedral prismatic crystals of forsterite, which are partly serpentinized in some cases. The interstices between forsterite crystals are filled with magnesioferrite

and perovskite (Figure 4e), as well as calcite. The latter often forms isometric cavities, and the walls of these cavities are covered with opaque minerals. As the rock reveals texture close to pegmatitic, the size of the cavities significantly increases. The walls of such cavities are covered with perovskite and magnesioferrite, coexisting with clintonite and minor clinocllore. Both oxide minerals form large crystals—up to 8 cm in size.

A paragenesis of perovskite, garnet, magnetite, clinocllore, and calcite was identified within coarse-grained chlorite-calcite veinlets. Small (up to 0.2 cm) grains of garnet, perovskite (Figure 4f), and magnetite were found directly in massive chlorite aggregates. Perovskite also occurs as inclusions in garnet (Figure 4g). In the central parts of veinlets, which mostly comprise coarse-grained calcite, larger crystals (up to 10 cm) of the same minerals occur.

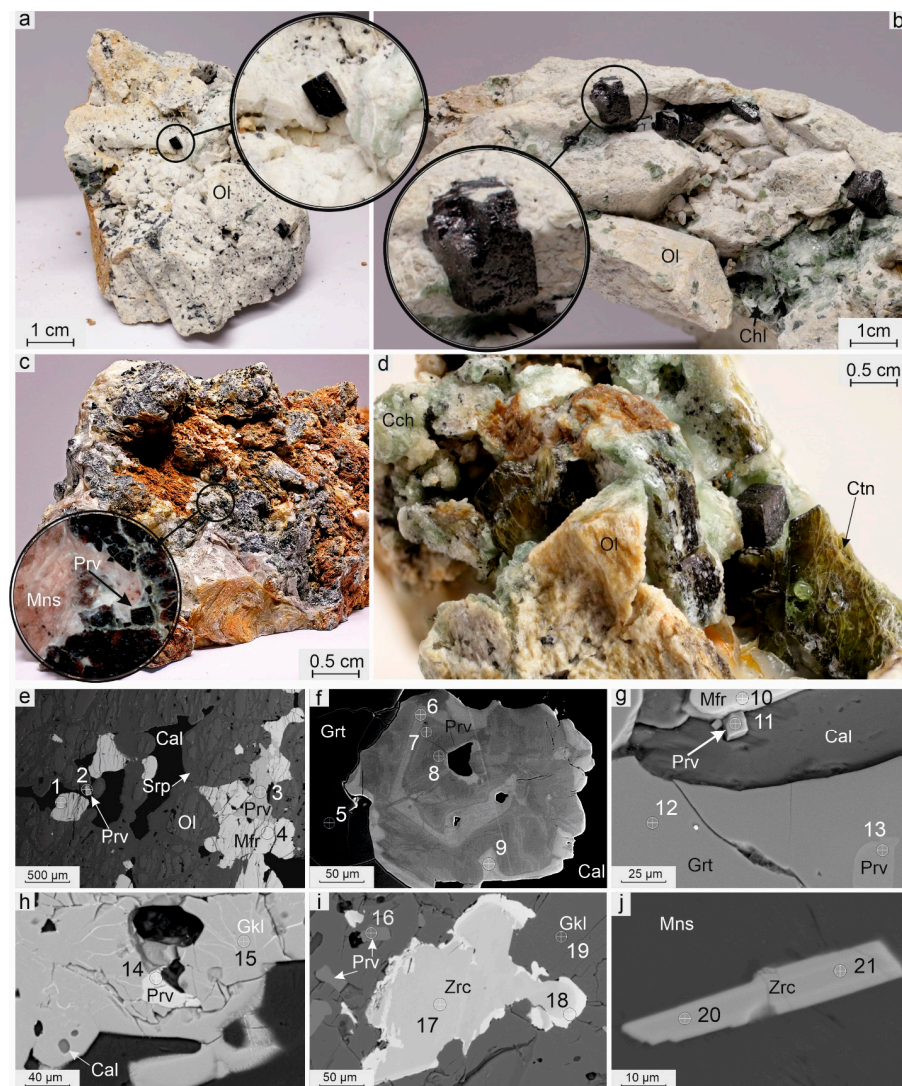


Figure 4. Parageneses with perovskite found in the Zelentsov Mine: (a,b)—small crystals of perovskite in fusion with olivine, (c)—an aggregate of perovskite and hydrotalcite-2H, (d)—a crystal of perovskite in aggregate of clinocllore, olivine and clintonite, (e–j)—SEM-photo in BSE mode. A circle with a crosshair indicates the analysis number in Table 1. Mineral symbols: Ol—olivine, Chl—chlorite, Cch—clinocllore, Ctn—clintonite, Mns—hydrotalcite-2H, Srp—serpentine, Cal—calcite, Prv—perovskite, Mfr—magnesioferrite, Grt—garnet, Gkl—geikielite, Zrc—zirconolite.

Table 1. Composition of minerals from perovskite parageneses of Zelentsov mine, wt %.

№	MgO	Al ₂ O ₃	SiO ₂	CaO	TiO ₂	V ₂ O ₅	MnO	FeO	Fe ₂ O ₃	Y ₂ O ₃	ZrO ₂	Ce ₂ O ₃	Nd ₂ O ₃	Sm ₂ O ₃	Σ	Mineral
1	17.11	0.59	—*	—	0.05	—	1.39	19.73	63.90	—	—	—	—	—	102.77	Mg _{0.79} Fe _{0.18} Mn _{0.04} Fe _{1.98} Al _{0.02} O _{4.00}
2	—	—	—	40.93	56.15	0.79	—	0.60	—	—	—	—	—	—	98.47	Ca _{1.01} Ti _{0.97} V _{0.01} Fe _{0.01} O _{2.98}
3	—	—	—	41.79	57.06	0.40	0.03	0.46	—	—	—	—	—	—	98.74	Ca _{1.00} Ti _{0.98} V _{0.01} Fe _{0.01} O _{2.99}
4	17.03	1.08	—	—	0.22	0.09	1.39	18.65	61.51	—	—	—	—	—	99.97	Mg _{0.80} Fe _{0.17} Mn _{0.04} Fe _{1.95} Al _{0.04} O _{4.00}
5	0.38	1.55	36.60	34.78	2.37	—	—	—	27.08	—	—	—	—	—	102.76	(Ca _{3.03} Mg _{0.05})Σ _{3.08} (Fe _{1.65} Al _{0.15} Ti _{0.14})Σ _{1.94} Si _{2.98} O _{12.02}
6	—	0.23	—	41.18	55.54	0.49	—	0.72	—	—	1.01	0.54	0.13	—	99.84	Ca _{1.00} Ti _{0.95} V _{0.01} Fe _{0.01} Al _{0.01} O _{2.97}
7	—	0.21	0.36	40.25	56.31	0.54	—	0.54	—	—	—	0.59	—	—	98.80	Ca _{0.99} Ti _{0.97} V _{0.01} Fe _{0.01} Al _{0.01} Si _{0.01} O _{2.99} *
8	—	—	0.41	41.04	56.41	0.54	—	0.46	—	—	—	0.48	—	0.31	99.65	Ca _{1.00} Ti _{0.97} V _{0.01} Fe _{0.01} Si _{0.01} O _{2.98} *
9	—	0.09	—	39.30	56.11	0.43	—	1.04	—	—	—	0.90	0.52	—	98.39	Ca _{0.98} Ti _{0.98} Fe _{0.02} V _{0.01} Ce _{0.01} O _{2.99}
10	13.02	—	—	0.73	—	—	2.14	22.61	61.15	—	—	—	—	—	99.65	Mg _{0.67} Fe _{0.28} Mn _{0.06} Ca _{0.03} Fe _{2.00} O _{4.00}
11	—	—	—	40.28	56.16	—	—	1.76	—	—	—	—	—	—	98.20	Ca _{0.99} Ti _{0.97} Fe _{0.03} O _{2.97}
12	0.33	2.40	36.05	34.71	2.79	—	—	—	26.07	—	—	—	—	—	102.35	(Ca _{3.03} Mg _{0.04})Σ _{3.07} (Fe _{1.61} Al _{0.17} Ti _{0.14})Σ _{1.92} Si _{2.94} O _{12.04}
13	—	—	—	40.81	56.01	—	—	0.27	—	—	—	0.32	—	—	97.41	Ca _{1.01} Ti _{0.98} Fe _{0.01} O _{2.98}
14	—	—	—	40.60	58.04	—	—	0.42	—	—	—	—	—	—	99.06	Ca _{0.99} Ti _{1.00} Fe _{0.01} O _{3.00}
15	30.45	—	—	—	64.24	0.85	1.94	2.24	—	—	—	—	—	—	99.72	Mg _{0.93} Ti _{0.99} Fe _{0.04} Mn _{0.03} V _{0.01} O _{3.00}
16	—	—	—	41.21	59.10	—	—	0.49	—	—	—	—	—	—	100.80	Ca _{0.99} Ti _{1.00} Fe _{0.01} O _{3.00}
17	—	1.09	—	12.39	36.16	—	—	—	6.28	2.59	34.36	1.01	1.55	0.34	95.77	(Ca _{0.81} Y _{0.08} Nd _{0.03} Ce _{0.02} Sm _{0.01})Σ _{0.95} Zr _{1.02} (Ti _{1.66} Fe _{0.29} Al _{0.08})Σ _{1.93} O _{6.94}
18	—	—	—	10.38	33.55	—	—	6.81	—	4.53	32.01	1.31	4.10	0.98	93.67	(Ca _{0.71} Y _{0.15} Nd _{0.09} Ce _{0.03} Sm _{0.02})Σ _{1.00} Zr _{1.00} (Ti _{1.62} Fe _{0.37})Σ _{1.99} O _{6.95}
19	29.54	—	—	—	65.00	—	1.42	4.42	—	—	—	—	—	—	100.38	Mg _{0.90} Ti _{1.00} Fe _{0.08} Mn _{0.02} O _{3.00}
20	—	—	—	8.00	31.96	—	—	0.02	6.76	7.63	32.80	2.27	5.37	1.96	103.53	(Ca _{0.56} Y _{0.26} Nd _{0.12} Ce _{0.05} Sm _{0.04} Fe _{0.04})Σ _{1.07} Zr _{1.04} (Ti _{1.56} Fe _{0.33})Σ _{1.89} O _{7.00}
21	—	—	—	7.64	32.03	—	—	0.88	5.49	7.28	32.58	2.96	6.14	1.61	102.10	(Ca _{0.54} Y _{0.25} Nd _{0.14} Fe _{0.08} Ce _{0.07} Sm _{0.04})Σ _{1.12} Zr _{1.04} (Ti _{1.57} Fe _{0.27})Σ _{1.84} O _{7.00}

Note. *—here and below content of element is below the detection limit. The analyses correspond to the point numbers in the Figure 4. *—the silicate matrix has been captured.

Paragenesis C was identified in sparse calcite-hydrothermalite-2H veins. These veins consist of medium-grained, tangled flakes of hydrothermalite-2H aggregate with subordinate calcite and geikielite. Perovskite primarily appears as inclusions within geikielite crystals (Figure 4h). Alongside perovskite, geikielite also hosts zirconolite inclusions (Figure 4i). Other zirconolite segregations are identified within hydrothermalite-2H matrix (Figure 4j).

At the Perovskite mine, perovskite was observed in three parageneses: perovskite-magnetite-clinocllore-calcite (D), perovskite-magnetite-clinocllore-clinohumite-calcite (E), and perovskite-magnetite-diopside-clinocllore-calcite (F) [18]. The most abundant is paragenesis D. The cubic perovskite crystals from this paragenesis are up to ca. 3 cm in size (Figure 5a). Perovskite typically forms close intergrowths with magnetite, observed in both fine-grained rocks and coarser, pegmatoidal aggregates.

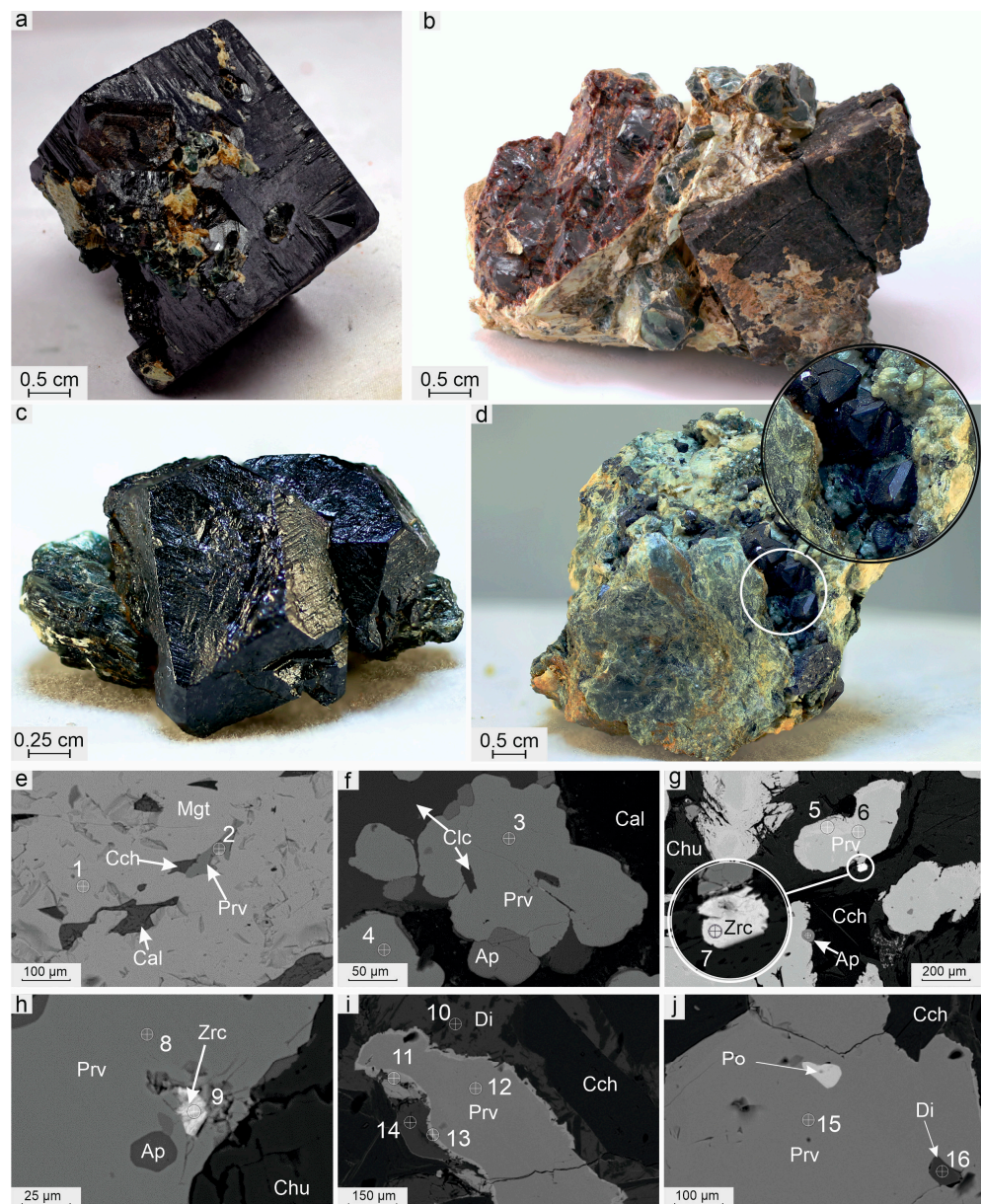


Figure 5. Parageneses of perovskite from the Perovskite Mine: (a)—perovskite crystal, (b)—clinohumite with perovskite and magnetites, (c)—fusion of magnetite crystals, (d)—magnetite and perovskite crystals in clinocllore aggregate, (e–j)—SEM-photo in BSE mode. Circle with a crosshair indicates the analysis number in Table 2. Mineral symbols: Chu—clinohumite, Cch—clinocllore, Di—diopside, Cal—calcite, Prv—perovskite, Mgt—magnetite, Ap—apatite, Zrc—zirconolite, Po—pyrrhotite.

Table 2. Composition of minerals from perovskite parageneses of Perovskite mine, wt %.

Nº	MgO	SiO ₂	CaO	TiO ₂	MnO	FeO	Fe ₂ O ₃	Y ₂ O ₃	Nb ₂ O ₅	ZrO ₂	La ₂ O ₃	Ce ₂ O ₃	Nd ₂ O ₃	Σ	Formulae
1	2.34	–	–	–	0.35	40.08	55.78	–	–	–	–	–	–	98.55	Fe _{0.86} Mg _{0.13} Fe _{2.00} O _{4.00}
2	–	–	40.20	56.73	–	1.97	–	–	–	–	–	–	–	98.90	Ca _{0.99} Fe _{0.04} Ti _{0.98} O _{2.98}
3	–	–	41.31	57.84	–	0.33	–	–	–	–	–	–	–	99.48	Ca _{1.01} Fe _{0.01} Ti _{0.99} O _{2.99}
4	–	–	40.78	57.51	0.09	0.37	–	–	0.19	–	–	–	–	98.94	Ca _{1.00} Fe _{0.01} Ti _{0.99} O _{2.99}
5	–	–	40.63	56.95	–	0.36	–	–	–	–	–	–	–	97.94	Ca _{1.00} Fe _{0.01} Ti _{0.99} O _{2.99}
6	–	–	39.84	56.61	–	1.40	–	–	–	–	–	–	–	97.85	Ca _{0.99} Fe _{0.03} Ti _{0.99} O _{2.99}
7	–	2.08	11.48	31.81	–	–	6.38	3.74	32.85	2.26	–	3.12	1.96	95.68	(Ca _{0.77} Y _{0.12} Ce _{0.07} Nb _{0.06} Nd _{0.4}) _{Σ1.06} Zr _{1.00} (Ti _{1.50} Fe _{0.30}) _{Σ1.80} Si _{0.13} O _{7.00} *
8	–	–	40.46	58.24	–	0.38	–	–	–	–	–	–	–	99.08	Ca _{0.99} Fe _{0.01} Ti _{1.00} O _{3.00} (Ca _{0.78} Y _{0.13} Ce _{0.06} Nb _{0.05} Nd _{0.3} La _{0.01} Mg _{0.06}) _{Σ1.13}
9	0.66	1.30	11.73	31.92	–	–	7.21	3.87	31.70	1.87	0.54	2.85	1.17	94.82	Zr _{0.96} (Ti _{1.49} Fe _{0.34}) _{Σ1.83} Si _{0.08} O _{6.90} *
10	18.18	54.01	26.03	0.14	–	0.15	–	–	–	–	–	–	–	98.51	Ca _{1.02} Mg _{0.99} Fe _{0.07} Si _{1.98} O _{5.98}
11	–	–	38.43	56.25	–	1.56	–	0.16	–	0.12	1.96	2.22	0.58	101.28	(Ca _{0.95} Fe _{0.03} Ce _{0.02} La _{0.02}) _{Σ1.02} Ti _{0.98} O _{3.00}
12	–	–	40.84	58.08	–	0.81	–	0.32	–	–	–	–	0.37	100.42	(Ca _{0.99} Fe _{0.02}) _{Σ1.01} Ti _{0.99} O _{2.99}
13	–	–	38.21	54.20	–	1.13	–	0.26	–	–	2.48	2.86	0.82	99.96	(Ca _{0.96} Fe _{0.02} Ce _{0.02} La _{0.02} Nd _{0.01}) _{Σ1.03} Ti _{0.96} O _{2.99}
14	18.38	54.58	26.05	–	–	1.08	–	–	–	–	–	–	–	100.09	Ca _{1.01} Mg _{0.99} Fe _{0.03} Si _{1.97} O _{5.97}
15	–	–	40.01	56.95	–	0.50	–	–	–	–	0.87	0.53	0.26	99.12	(Ca _{0.99} Fe _{0.01} La _{0.01}) _{Σ1.01} Ti _{0.99} O _{2.99}
16	16.96	52.76	25.61	–	–	2.24	–	–	–	–	–	–	–	97.57	Ca _{1.02} Mg _{0.94} Fe _{0.07} Si _{1.97} O _{5.97}

Note. The analyses correspond to the point numbers in the Figure 5. *—the silicate matrix has been captured.

In the paragenesis E, perovskite is a rock-forming mineral, constituting up to 5 vol. % of the rock. Perovskite occurs as relatively large cubic or, less frequently, rhombododecahedron crystals (Figure 5b,c). It is often associated with fluorapatite (Figure 5f) and zirconolite (Figure 5g,h).

In the paragenesis F, perovskite mainly forms crystals of complex habits, typically octahedrons (Figure 5d) or tetracubes. Particularly, crystals from this paragenesis, often exhibit a zonal structure (Figure 5i), which is attributed to the uneven distribution of minor elements such as Nb, Yb, and REE. In rare cases, perovskite from this assemblage contains sulfide inclusions, mostly pyrrhotite (Figure 5j).

All of the mineral parageneses described are presented both fine- and coarse-grained aggregates. The large crystals of magnetite (up to 8 cm), perovskite (up to 5 cm), and clinocllore (up to 15 cm) incrustated the cavity walls. The size of investigated crystals of perovskite was suitable for goniometric measurements carried out to evaluate the diversity of perovskite crystal morphology from different mines (Figure 6).

4.2. Perovskite Crystal Shape Difference between Mines

All studied perovskite crystals exhibit twinning. The twin structure of natural perovskites is a result of a phase transition from the cubic to the orthorhombic system [14,19]. This structure is visible in cross-polarized transmitted light (Figure 6a–c). Perovskites show distinct anisotropy and minor birefringence, characteristic of the orthorhombic system. At the same time, the angles between crystal facets are the same as for the hexoctahedral class of the cubic system. Hence, polyhedrons like the cube, octahedron, and rhombododecahedron from the cubic system are adopted, following the precedent set in the classic crystallographic atlas [20].

The most common perovskite form is the cube {100}. Alongside the cube, the octahedron {111} and rhombododecahedron {110} facets are also frequently observed. Crystals with such facets were found in all mines and nearly all parageneses. However, perovskites predominantly shaped as octahedrons {111}, rhombododecahedrons {110}, and tetracubes {320} are much less abundant; only in the Perovskite mine, a single crystal of such shape was found. The biggest diversity of crystal shapes is observed for perovskites from the Perovskite and Akhmatov mines [14]. A complicated combination of octahedrons {111}, rhombododecahedrons {110}, several tetracubes {210}, {320}, {730}, {520}, tetragonal trisoctahedrons {211}, trigon trisoctahedrons {221}, and rare hexoctahedrons {543} are typical for perovskites from the perovskite-magnetite-clinocllore-clinohumite-calcite and perovskite-magnetite-diopside-clinocllore-calcite parageneses of the Perovskite mine.

4.3. Chemical Composition of Perovskites

EPMA revealed a homogeneous structure and an almost complete lack of minor elements (other than Fe) in most individual perovskite crystals. The composition closely approximates the stoichiometric formula CaTiO_3 , especially in the larger crystals from mineralized Carboniferous cavities. Additionally, some perovskites display a distinct zonal structure characterized by variations in iron content across different zones.

Small perovskite grains (<1 sm) may also exhibit distinct zonality, which appears to be controlled by the sequential interchange of zones enriched or depleted in both Fe and minor elements (Y, Nb, REE; Figure 7a–d). In backscattered electron images, these brighter zones are enriched in Y, Nb, and REE. Although there is no consistent compositional trend towards the outer parts of the crystals, the outermost zones frequently show the highest enrichment in rare components. In some instances, perovskite compositions exceeding 5 wt. % of (Y+Nb+REE) are found altering the outermost layers of nearly pure crystals.

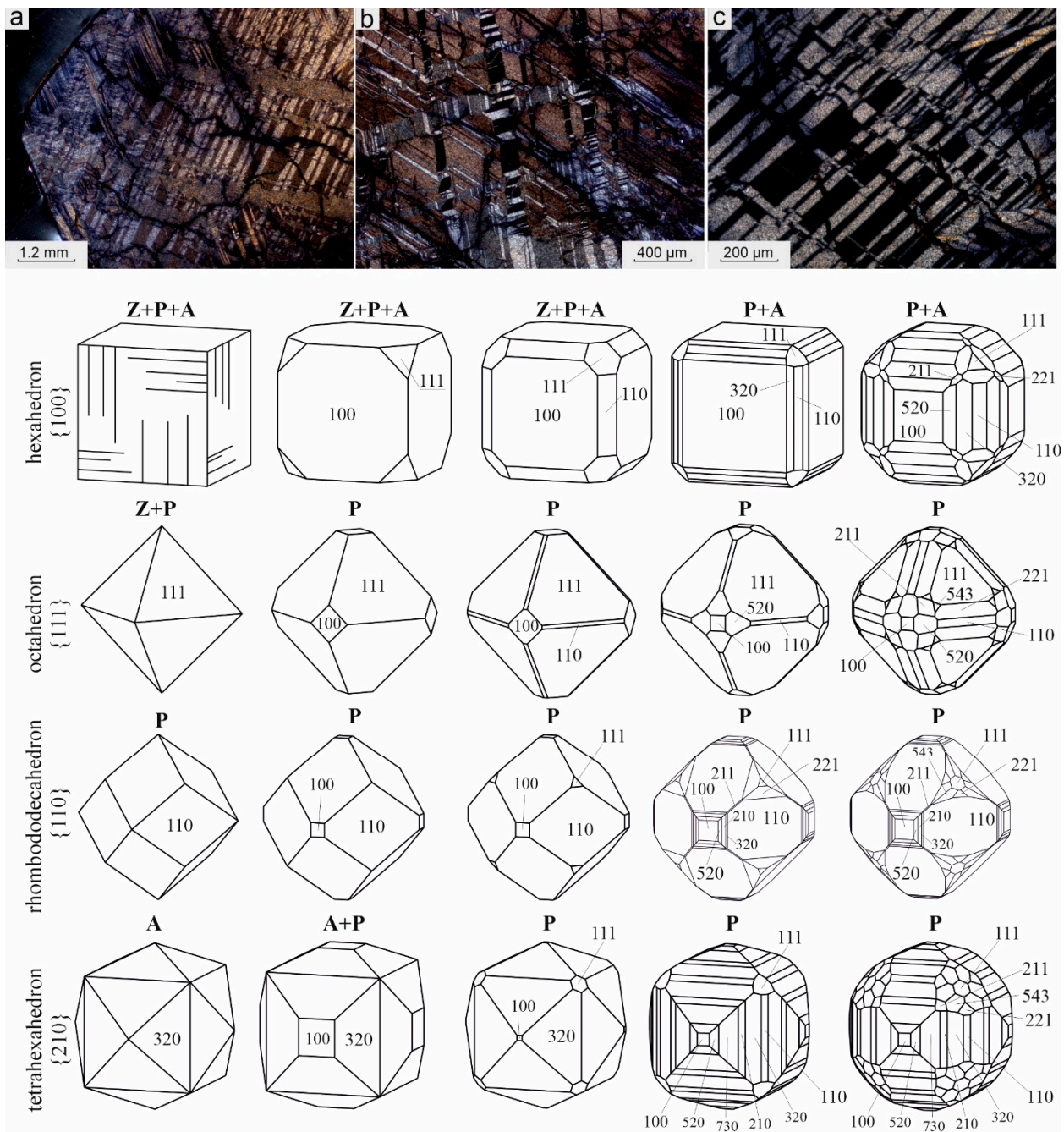


Figure 6. The shape of studied perovskite crystals. The letter above the graphics indicates the locality for which the shape was observed: Z—Zelentsov Mine, P—Perovskite Mine, A—Akmatov Mine. Authors’ material is used for Zelentsov and Perovskite Mine, while the investigations from references [14,20] were adopted for Akhmatov Mine. (a–c)—twinning of perovskite crystals is in cross-polarized transmitted light.

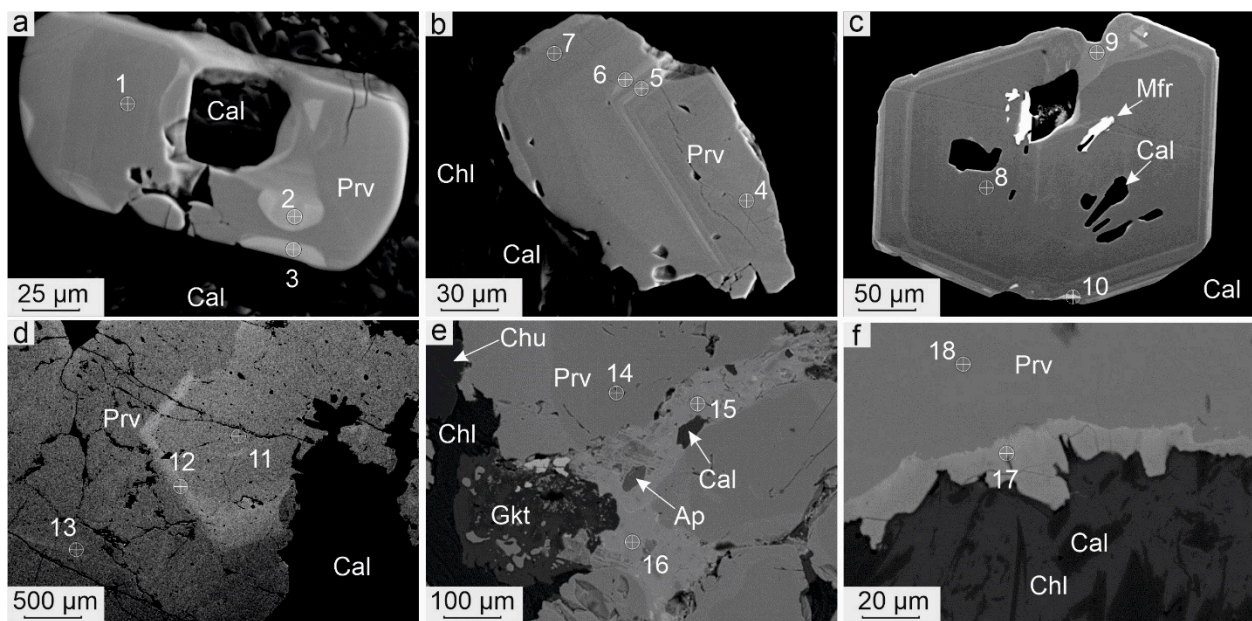


Figure 7. Inhomogeneous structure of perovskite grains defined by trace elements content variation: (a–d)—zonal crystals, (e,f)—perovskite substitution by newly-formed REE and another trace elements-enriched perovskite. A circle with a crosshair indicates the analysis number in Table 3.

Analysis of perovskite, EPMA results (427 analyses in 79 crystals), revealed that the perovskite from the perovskite-magnetite-clinocllore-calcite paragenesis of the Perovskite mine contains almost no minor elements excluding Fe (average content ~ 0.35 wt. % of elements). A similar minor element profile is observed in perovskites from the paragenesis A of the Zelentsov mine. The most REE-enriched perovskites are those from the perovskite-magnetite-clinocllore-clinohumite-calcite and perovskite-magnetite-clinocllore-calcite parageneses (Figure 8a). The highest LREE concentrations are observed in crystals of complicated habit composed of an octahedron, rhombododecahedron, tetracube, and other forms. The highest Nb and Y contents are inherent to perovskite from paragenesis C and perovskite-magnetite-clinocllore-clinohumite-calcite parageneses. Perovskites from the Zelentsov mine consistently exhibit higher vanadium content (Figure 8b), likely due to the adjacent vanadium-rich titanomagnetite ores. In summary, no clear regularity in impurity distribution among perovskites of different types and localities was observed. However, perovskites with more complex habits demonstrate higher enrichment in REE, Y, and Nb compared with other perovskites.

Trace element distribution was analyzed using LA-ICP-MS. All perovskites exhibited a negative REE spectrum slope, with a consistent decrease from lighter to heavier elements. Octahedral perovskites in carbonate-mineralized cavities of the Perovskite mine showed a slightly lower REE content compared to cubic crystals from the same location (Table 4, Figure 9). The lowest total REE was observed in carbonate cavities from perovskite-magnetite-forsterite-calcite rocks at the Zelentsov mine. The LREE profile of the studied perovskites is compatible with that of ultramafic alkaline rocks, and the HREE profile aligns with that found in kimberlites (Figure 9). Additionally, small < 0.5 sm metasomatic perovskite grains from the garnet-vesuvianite skarn at the Akhmatovaskaya mine were analyzed for comparison [14]. These analyses of grains are characterized with significant REE depletion, with levels often near the mass spectrometer's detection limit, producing a sawtooth-shaped curve (Figure 9).

Table 3. Perovskite composition from different parageneses of Perovskite and Zelentsov mines, wt %.

Nº	CaO	TiO ₂	V ₂ O ₃	FeO	La ₂ O ₃	Ce ₂ O ₃	Nd ₂ O ₃	Sm ₂ O ₃	Σ	Formulae
1	40.75	57.13	0.35	0.37	–	0.83	–	–	99.44	(Ca _{1.00} Fe _{0.01} Ce _{0.01}) _{Σ1.01} (Ti _{0.98} V _{0.01}) _{Σ0.99} O _{2.99}
2	37.82	54.33	0.62	2.06	–	2.42	2.03	0.23	99.51	(Ca _{0.95} Fe _{0.04} Ce _{0.02} Nd _{0.02}) _{1.03} (Ti _{0.96} V _{0.01}) _{0.97} O _{2.98}
3	38.16	54.61	0.54	1.76	–	2.88	1.74	–	99.69	(Ca _{0.96} Fe _{0.03} Ce _{0.02} Nd _{0.01}) _{1.03} (Ti _{0.96} V _{0.01}) _{0.97} O _{2.99}
4	40.53	57.40	0.50	0.68	–	0.73	–	0.21	100.05	(Ca _{0.99} Fe _{0.01} Ce _{0.01}) _{1.01} (Ti _{0.98} V _{0.01}) _{0.99} O _{2.98}
5	38.79	55.63	0.32	1.57	–	1.42	0.26	–	98.15	(Ca _{0.97} Fe _{0.03} Nb _{0.02} Ce _{0.01}) _{1.03} (Ti _{0.98} V _{0.01}) _{0.99} O _{2.98}
6	39.40	56.05	0.37	1.43	–	1.52	0.65	0.19	99.60	(Ca _{0.97} Ce _{0.01} Fe _{0.03} Nd _{0.01}) _{1.02} (Ti _{0.97} V _{0.01}) _{0.98} O _{2.98}
7	39.39	56.55	0.62	0.66	–	0.71	–	–	97.92	(Ca _{0.98} Fe _{0.01} Ce _{0.01}) _{1.00} (Ti _{0.99} V _{0.01}) _{1.00} O _{2.98}
8	40.80	57.31	0.38	0.41	–	0.75	–	–	99.66	(Ca _{1.00} Fe _{0.01} Ce _{0.01}) _{1.02} (Ti _{0.98} V _{0.01}) _{0.99} O _{2.99}
9	39.53	56.77	0.84	0.67	–	0.66	0.69	–	99.15	(Ca _{0.98} Fe _{0.01} Ce _{0.01} Nd _{0.01}) _{1.00} (Ti _{0.98} V _{0.02}) _{1.00} O _{2.98}
10	37.29	55.38	–	1.75	–	2.35	1.26	0.16	98.19	(Ca _{0.95} Fe _{0.03} Ce _{0.02} Nd _{0.01}) _{1.01} (Ti _{0.99} V _{0.00}) _{0.99} O _{2.98}
11	40.38	57.50	–	0.66	0.36	0.43	–	–	99.33	(Ca _{0.99} Fe _{0.01}) _{1.01} (Ti _{0.99} V _{0.00}) _{0.99} O _{2.98}
12	39.85	56.72	–	0.77	–	0.75	–	–	98.09	(Ca _{0.99} Fe _{0.01} Ce _{0.01}) _{1.01} (Ti _{0.99} V _{0.00}) _{0.99} O _{2.98}
13	40.12	56.61	–	0.48	–	0.27	–	–	97.48	(Ca _{1.00} Fe _{0.01}) _{1.01} (Ti _{0.99} V _{0.00}) _{0.99} O _{2.99}
14	39.90	57.20	–	0.48	–	–	–	–	97.57	(Ca _{0.99} Fe _{0.01}) _{1.00} (Ti _{1.00} V _{0.00}) _{1.00} O _{2.98}
15	38.43	56.85	0.31	1.70	0.70	2.51	0.40	–	100.89	(Ca _{0.95} Fe _{0.03} Ce _{0.02} La _{0.01}) _{1.01} (Ti _{0.98} V _{0.01}) _{0.99} O _{2.98}
16	38.38	56.68	0.32	1.66	0.62	2.55	0.36	–	100.58	(Ca _{0.95} Fe _{0.03} Ce _{0.02} La _{0.01}) _{1.01} (Ti _{0.98} V _{0.01}) _{0.99} O _{2.98}
17	37.33	54.91	–	1.39	1.04	3.06	0.38	–	98.12	(Ca _{0.95} Ce _{0.03} Fe _{0.03} La _{0.01}) _{1.02} (Ti _{0.98} V _{0.00}) _{0.98} O _{2.98}
18	39.76	58.60	–	0.66	0.15	0.28	–	–	99.45	(Ca _{0.98} Ce _{0.00} Fe _{0.01}) _{0.99} (Ti _{1.01} V _{0.00}) _{1.01} O _{2.98}

Note. Formulae are calculated per 3 atomic of oxygen. Analys 5 includes 0.16 wt. % of Nb₂O₅.

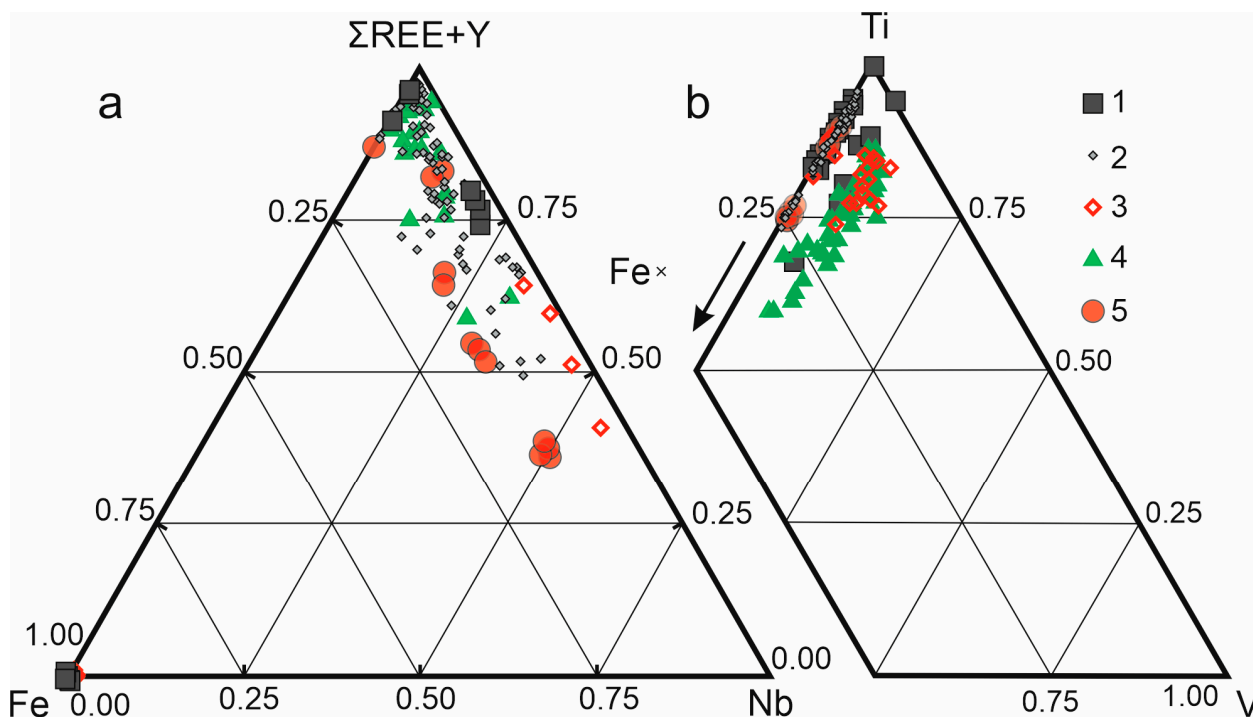


Figure 8. Ternary diagrams of Fe-Nb-REE (a) and Fe-Ti-V (b) content in perovskite from different parageneses of the Perovskite and Zelentsov Mines (Table 4): 1—octahedral crystals from perovskite-magnetite-diopside-chlorite-calcite parageneses (Perovskite Mine), 2—cubic crystals from perovskite-magnetite-clinocllore-calcite paragenesis (Perovskite Mine), 3—cubic crystals from paragenesis A, 4—perovskite from skarns of Akhmatov Mine [18], 5—field of REE content in perovskites of Perovskite Mine [18].

Table 4. The content of impurity elements in perovskites from Perovskite and Zelentsov mines according to the results of LA-ICP-MS, ppm.

Element	Octahedral Perovskites of Perovskite Mine					Cubic Perovskites of Perovskite Mine				Cubic Perovskites of Zelentsov Mine			
	№	1	2	3	4	5	6	7	8	9	10	11	12
Fe	2390	2800	3790	2620	3680	4240	3400	4070	2830	2410	2950	2550	
Sr	57.0	57.70	55.7	53.20	52.1	62.6	52.0	53.0	29.2	22.2	20.5	39.80	
Y	216	217.00	38.9	143.7	231	179	316	320	470	224	194	329	
Zr	12.0	12.0	8.59	22.1	24.8	21.5	26.7	27.7	345	293	56.0	622	
Nb	466	469	624	479	334	557	237	312	138.5	139	249	166	
La	3320	3360	4760	2950	2260	3440	1770	2280	798	352	1550	510	
Ce	5190	4720	8560	4000	3250	4370	2760	3430	1430	906	2530	493	
Pr	463	480	735	341	327	407	292	322	153.6	116.6	251	45.9	
Nd	895	903	1335	644	696	786	682	808	306	257	438	82.0	
Sm	444	402.4	495	451	563	624	580	712	270	227	225	70.8	
Eu	110.5	111.9	111.0	148.0	143	175	135	161	71.0	43.3	43.2	22.0	
Gd	199.0	195	167.0	290.0	391	341	387	390	269	184	169	67.6	
Tb	20.1	20.2	11.2	28.40	40.2	31.9	39.1	40.1	37.9	25.0	20.2	12.8	
Dy	94.2	98.2	40.9	123.0	179	137	187	195	253	146.9	115	91.0	
Ho	11.1	10.9	2.84	9.73	15.7	11.6	17.8	19.8	26.8	15.4	12.1	13.8	
Er	35.8	36.3	8.60	36.2	64.2	42.5	73.8	72.4	138.5	76.1	59.3	93.0	
Tm	2.18	2.19	0.37	1.60	2.37	1.69	3.03	3.39	7.52	3.75	3.12	6.44	
Yb	10.6	11.0	11.3	7.17	11.5	7.34	14.9	16.1	44.1	22.3	14.7	45.7	
Lu	0.81	0.78	0.13	0.59	0.89	0.54	1.06	1.18	2.91	1.65	0.97	3.94	
Pb	18.0	18.0	24.0	16.1	–	16.0	12.3	15.2	1.32	0.77	3.51	4.69	
La/Yb	313	305	422	411	197	469	119	142	18	16	105	11	

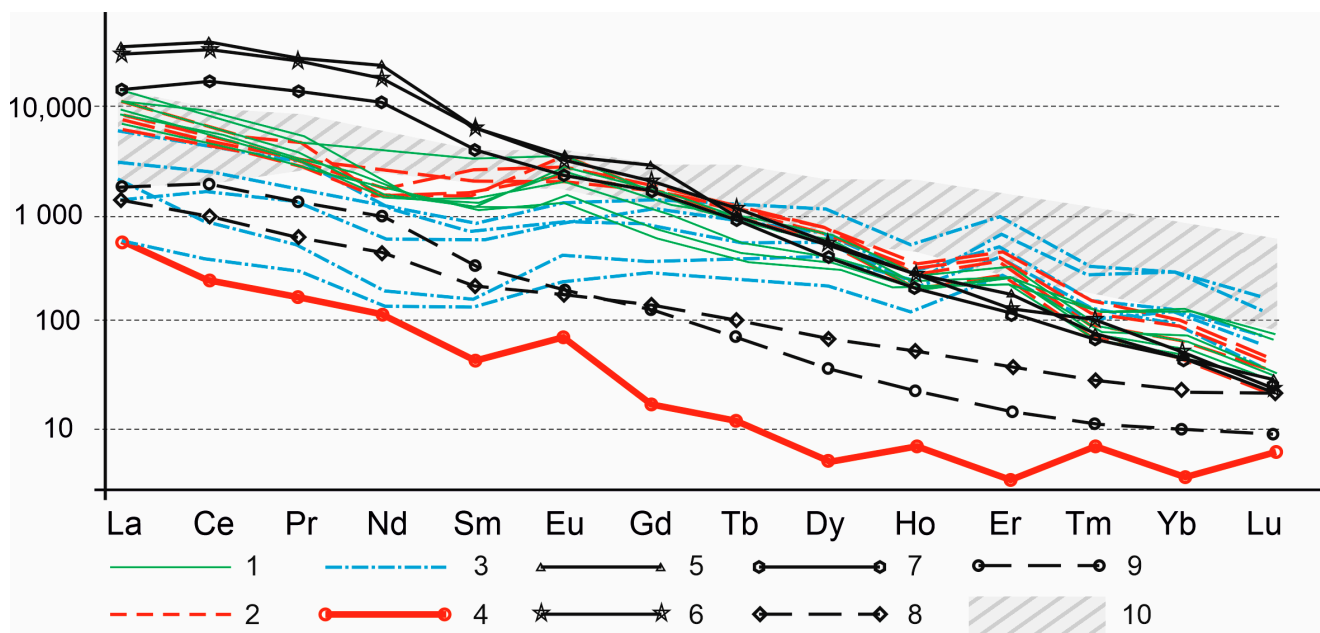


Figure 9. LA-ICP-MS C1-chondrite-normalized REE-distribution patterns [21]: 1—octahedral crystals from perovskite-magnetite-diopside-chlorite-calcite parageneses (the Perovskite Mine; our data), 2—cubic crystals from perovskite-magnetite-clinocllore-calcite paragenesis (the Perovskite Mine; our data), 3—cubic crystals from paragenesis A (our data), 4—perovskite from skarns of Akhmatov Mine [18], 5–7—kimberlitic perovskites: 5—Udachnaya Pipe, Russia [9], 6—Chicken Park pipe, Colorado, USA [9], 7—Kuruman, South Africa [22], 8, 9—from alkaline pyroxenites of Africanda complex, Kola Peninsula, Russia [23], 10—field of REE content in perovskites of Perovskite Mine [18].

4.4. U-Pb Age of Perovskite Mineralization

The results of U-Pb SHRIMP-II analyses of perovskites are presented in Figure 10. The current U/Pb ratio dispersion allows for plotting a total polychron revealing an upper intercept at 535 ± 43 Ma with an MSWD = 0.5 (Figure 10a). When plotting distinct concordant clusters, much lower error and significant differences in perovskite ages can be observed. For instance, the age of octahedral perovskites from the Perovskite mine is 532 ± 2 Ma (Figure 10b), the age of cubic perovskites from the same mine is 497 ± 4 Ma (Figure 10c), and the age of perovskites from clintonite-magnetite-forsterite-calcite rocks of Zelentsov mine is 486 ± 6.4 Ma (Figure 10d).

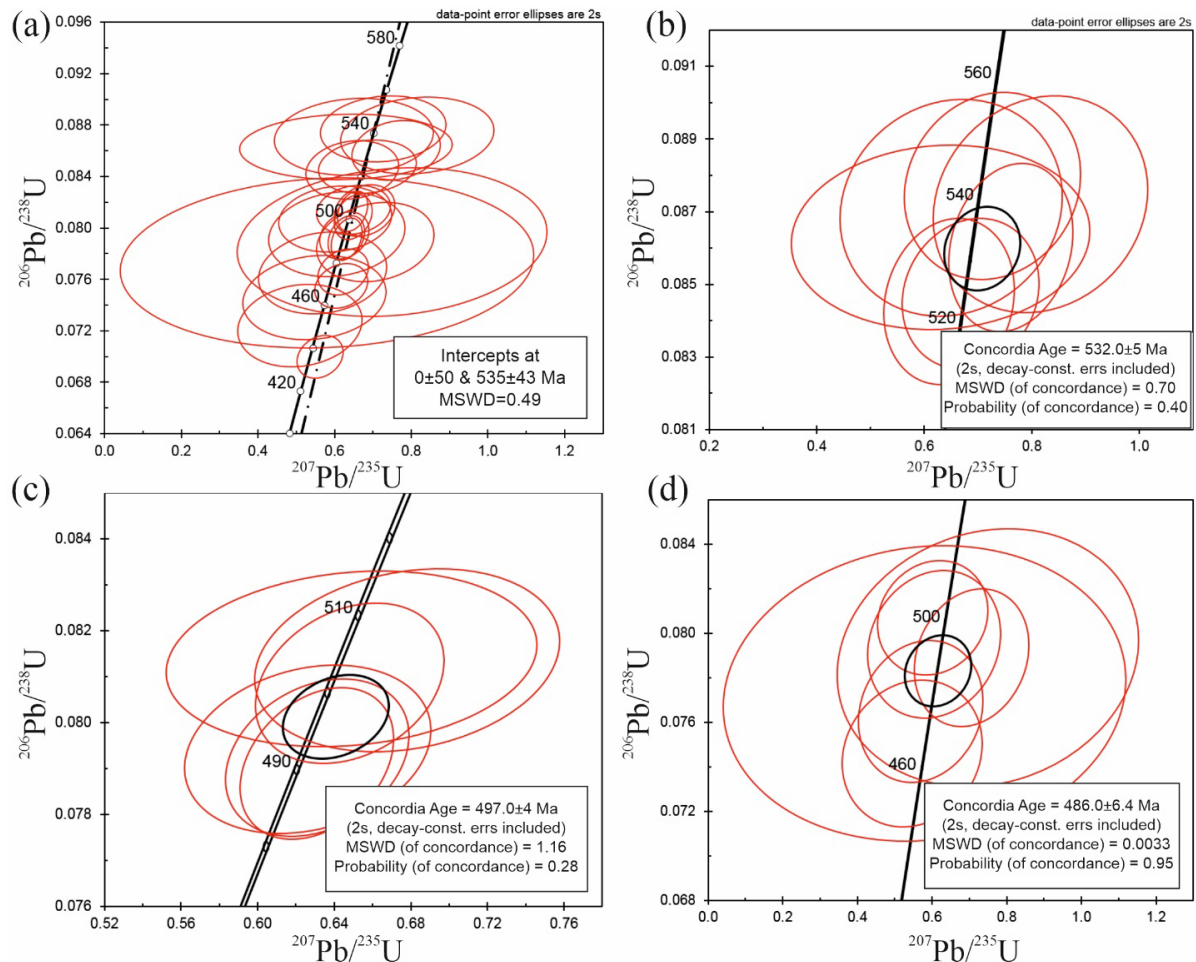


Figure 10. $^{206}\text{Pb}/^{238}\text{U}$ — $^{207}\text{Pb}/^{235}\text{U}$ diagrams concordia for perovskites of mines spatially related to the Kusinsko-Kopanskaya layered intrusion [21] (a) and opened by individual excavations at Perovskite (b,c) and Zelentsov Mines (d).

5. Discussion

5.1. Comparison of Perovskite from Calcite-Silicate Veins and Ultramafic Alkaline Rocks

One of the prominent issues regarding perovskite mineralization at its type locality concerns the origin of perovskite-enriched carbonate vein rocks closely associated with the Kusinsko-Kopanskaya layered intrusion. The perovskite mineralization studied here is unique both in terms of enormous crystal sizes (Figure 5) and their abundance, thus differing from typical perovskite occurrences. Naturally occurring perovskite may be found in skarns [24–26], carbonatites [10,27,28], kimberlites [8,9,16,29–31], and more broadly, is a typical accessory mineral of mafic and ultramafic silica-undersaturated rocks [6,10]. The origin of such unusual mineralization demands critical revision and explanation, which should be based on textural evidence, comparison of studied perovskites with those from other types of objects in terms of chemical composition, and the relationship between perovskite-bearing calcite veins and the Kusinsko-Kopanskaya layered intrusion.

The perovskites within the carbonate rocks display significant chemical differences compared to those in silica-undersaturated alkaline ultramafic rocks, carbonatites, and skarns. To illustrate, perovskites from alkaline ultramafic rocks are typically enriched in Nb, Y, and Sr [28,31,32]. Similar chemical features are also characteristic of perovskites in kimberlites [6,8,9,33], and similar levels of trace elements were reported for perovskites in skarns of the Tazheran complex. On the other hand, the Sr content in perovskites from South Urals Mineral Mines is notably low, barely exceeding 48 ppm, and they show a

pronounced depletion in U and Th compared to their counterparts in alkaline-ultramafic rocks, as depicted in Figure 11.

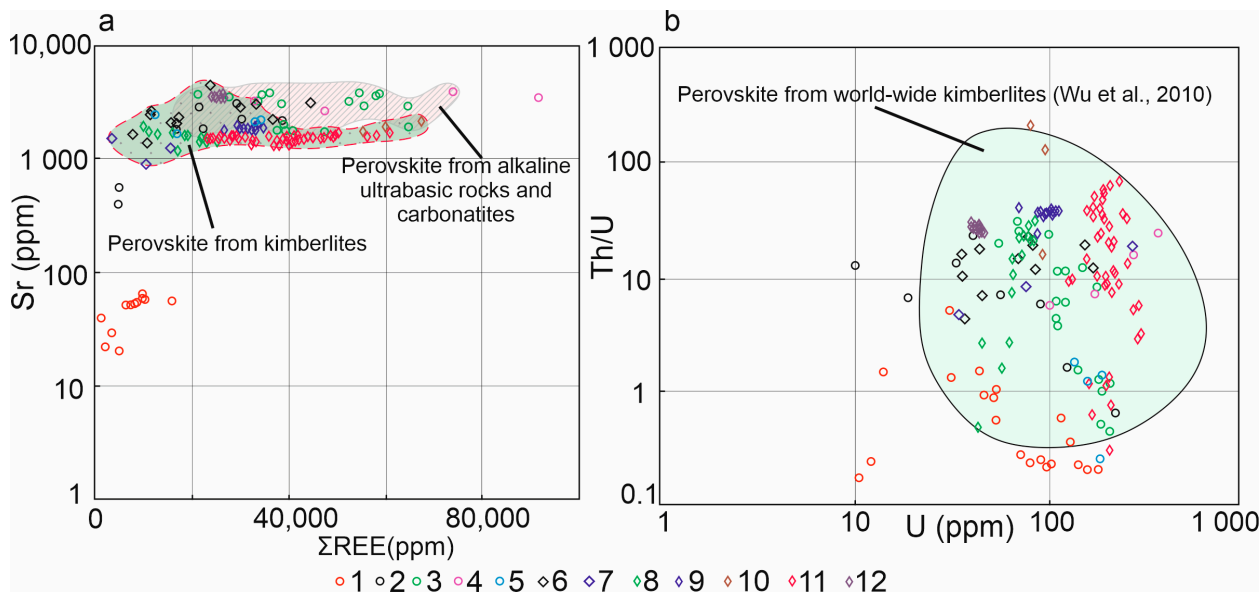


Figure 11. Comparison of studied perovskites composition with composition of perovskites from kimberlites and alkaline ultramafic rocks in Sr-REE (a) and Th/U-U (b) coordinates: 1—perovskites of the Perovskite and Zelentsov Mines, 2—Kola Peninsula, Afrikanda and Vuojarvi complexes [28], 3—Oka complex [32], 4—Afrikanda complex [31], 5—carbonatites and foscortite of the Guli complex, Siberia [34], 6—Eastern Dhawar kimberlite [33], 7—Premier pipe kimberlite [8], 8—Chicken Park kimberlite [9], 9—Iron Mountain kimberlite [9], 10—Grizzly pipe [9], 11—Udachnaya East kimberlite [9], 12—katungite from Bunyeruguru [9].

The elemental distribution within the perovskites diverges from those observed in ultramafic alkaline rocks. The latter are typically characterized by perovskites enriched in LREE, Sr, Nb, and Th across all generations, with a potential transition to loparite in later stages [28,32,35]. The studied perovskites predominantly exhibit a depleted inner core that has an abrupt transition to enriched zones (Figure 7a,c) or exhibit an inverse pattern (Figure 7b,d). Nonetheless, a holistic analysis of the mineral occurrences, rather than focusing solely on individual grains, reveals that the octahedral, rhombododecahedral, and tetrahedral perovskites from the earliest parageneses are notably enriched in LREE, Sr, Nd, and Th. This zoning pattern resembles the “normal zoning” concept as delineated in [30].

Another feature of the studied perovskites is the presence of outer rims that in some cases are enriched in REE (Figure 7e,f). Textural observations strongly indicate that these zones are of late origin, as they overgrow the primary REE-poor perovskite and even form fractures within it (Figure 7e). This phenomenon bears a striking similarity to the reverse zoning observed in perovskites from the Lac de Gras kimberlites, as elucidated by Chakhmouradian and Mitchell [9].

In summary, the perovskites studied in this research differ from those found in kimberlites and other alkaline and ultramafic rocks by having lower concentrations of REEs and lower LREE/HREE ratios.

5.2. The Nature of Perovskite Mineralization and Its Geological Implications

Currently, three models explain the formation of perovskite mineralization: the “skarn” model, which suggests that mineralization occurs through magnesian skarns at the contact between the Kusinsko-Kopanskaya intrusion and dolomites [11]; the “metamorphogenic” model, proposing that perovskite mineralization results from regional metamorphism [12];

and the “carbonatite” model, which associates it with endogenous activity on the Western slope of the Southern Urals [13,14,18]. Recent U-Pb dating of perovskites from mineral mines, showing ages between 486–535 Ma [18], along with earlier TIMS dating results, contrasts sharply with the age of the Kusinsko-Kopanskaya intrusion (1379 ± 8 Ma [15]). This significant age disparity casts doubt on the “skarn” model and points to the need for an alternative explanation for perovskite mineralization.

The age of the perovskites, determined through U-Pb dating from various mineral mines, ranges from 486–535 Ma. This aligns with previously acquired TIMS ages for perovskites [12], but markedly contrasts with the age of the Kusinsko-Kopanskaya intrusion, suggesting limitations in the traditionally posited “skarn” model and necessitating the exploration of an alternative explanation for its genesis.

Gekimyants [12] proposed a metamorphic hypothesis for the formation of perovskite mineralization, suggesting that the interaction between dolomites and limestones of the Satka Formation (R1) with the Kusinsko-Kopanskaya intrusion led to the formation of calciphyres and magnesian skarns with varying rock compositions, such as forsterite, phlogopite, and spinel. These formations reach maximal thicknesses of 2 m and 0.5 cm, respectively. Under garnet-amphibolite facies conditions, gabbroids and initial magnesian skarns underwent metamorphism, giving rise to metamorphogenic coarse-grained ilmenite-magnetite ores and fostering the emergence of titanium-rich magnesian skarns, including titanium-bearing clinohumite and chondrodite, högbomite, ludwigite, and calcareous garnet-amphibole-salite skarns. These transformations are hypothesized to have been induced by the intrusion of an unseen granite pluton akin to the Berdyash massif [12].

The Kusinsko-Kopanskaya intrusive rocks, magnesian and calcareous skarns, and the host carbonate rocks of the Satka Formation were all influenced by epigenetic regional metamorphism. This process led to the formation of several secondary minerals in gabbroids-albite, chlorite, epidote, axinite-(Fe), pumpellyite, calcite, and titanite. In titanomagnetite ores, pyrite, vallerite, and tochilinite emerged, while the carbonate rocks of the Satka Formation underwent partial replacement by serpentine and brucite. The early magnesian and calcareous skarns are also altered by low-grade metamorphism, resulting in the appearance of diverse minerals and mineral associations such as tremolite-clinoclone (from fassaite skarns), clinoclone with hydrotalcite-2H, perovskite, magnetite, hematite, and iron-free diopside (from spinel-forsterite skarns with Ti-bearing clinohumite). Alpine-type veins formed after skarns, indicative of low-grade metamorphism, were observed with the subsequent mineral assemblages compared by Gekimyants to rodingites. In the study [12], correlations between the conditions facilitating perovskite mineralization in the Nazyamsky mountains and the rodingites at the Saranovskoye deposit were established.

Prior to developing the metamorphogenic model for perovskite mineralization, several researchers revisited data on the Kusinsko-Kopanskaya intrusion and its contacts [36]. Their findings confirmed that all mineral mines within the Nazyamsky mountains are situated amidst ortho-amphibolites after gabbro, with the intrusion contacts described as “cold,” suggesting no direct rock/magma interaction. These discoveries, along with structural-mineralogical and ontogenic studies, led to the proposition of a “carbonatite” hypothesis to explain the origin of perovskite mineralization [13].

Based on the data analysis, the diopside-andradite rocks were classified as precarbonatite skarns, commonly reported in ultrabasic alkaline complexes with carbonatites of the Kola Peninsula and North Karelia [27]. In the mineral mines of the Nazyam Mountains, indicator minerals such as titanium-bearing varieties of clinohumite, chondrodite, vesuvianite, and andradite were identified [11], etc. Calcareous skarns give rise to polychronous carbonatites of the albite-calcite facies, which typically feature minerals associated with carbonatites, including zircon, perovskite, calzirtite, phlogopite, allanite-(Ce), baddeleyite, and manganese picroilmenite. The low concentrations of Nb in Ti-Zr minerals and perovskite are attributed to their association with the early (barren) carbonatites of the albite-calcite facies. Similar characteristics in carbonatites have also been documented in the Ufalei metamorphic block [13].

The “skarn” model appears inapplicable to the formation of perovskite mineralization due to a pronounced age discrepancy between the perovskites and the Kusinko-Kopanskaya intrusion. The “metamorphogenic” model, although detailed, does not fully account for the observed phenomena. Conversely, the “carbonatite” model gains credibility from similarities between the composition of perovskites from the mineral mines of the Nazyamsky Mountains and those found in traditional carbonatites associated with alkaline intrusions, further supported by the presence of rare minerals typically found in carbonatites. Additionally, the distribution of trace elements in perovskites questions their derivation from low-temperature processes, as it is highly unlikely for low-temperature perovskites to chemically resemble those found in kimberlites or alkaline ultramafic rocks, especially given the varying metamorphic grades along the Kusinko-Kopanskaya intrusion, where the northern parts show significant metamorphism unlike the southern parts, yet calcite-silicate veins with perovskite mineralization are consistently present. The investigated silicate-carbonate veins, bearing perovskite mineralization, should not be directly equated with conventional mantle carbonatites but might better be described as carbonatite-like dikes or crustal carbonatites, following theories proposing their formation through the melting of crustal carbonates upon contact with syenite magma in the presence of water. This discussion, while beyond the scope of this paper, is supported by recent findings of endogenous activity on the western flank of the Southern Urals. Zircon age determinations from the subalkaline basaltoids of the Navysh (R1), Ai (R1), Mashak (R2), and Igonin (R3) formations reveal a relatively constrained age span of 435–455 Ma, suggesting a magmatic origin as detailed in source [37,38], which enhances the “carbonatite” model and allows us to consider it a plausible explanation for the genesis of perovskite mineralization.

6. Conclusions

Six mineral parageneses have been identified in the carbonate rocks excavated by the Zelentsov and Perovskite mines. These can be sequentially arranged based on their mineral assemblages and corresponding temperatures, from high to low: perovskite-magnesioferrite-forsterite-calcite (A) → perovskite-magnetite-diopside-clinocllore-calcite (F) → perovskite-clinocllore-clinohumite-calcite (E) → perovskite-garnet-magnetite-clinocllore-calcite (B) = perovskite-magnetite-clinocllore-calcite (D) → perovskite-spinel-hydrocalcite-2H-calcite (C). Early high temperature parageneses feature perovskites with complex shapes dominated by octahedrons, rhombododecahedrons, and tetrahedrons. As the mineralization temperature decreases, rhombododecahedral perovskites are progressively replaced by octahedral and cubic forms. This morphological evolution is accompanied by changes in chemical composition: during the initial high-temperature stage, trace elements predominantly accumulate in octahedral, rhombododecahedral, and tetrahedral perovskites, while subsequent stages see minerals rich in Zr, Y, REE, and other trace elements crystallizing, often with the outer margins of perovskite becoming enriched in Y, Nb, and REE.

Compositional analysis and age determination suggest that perovskites within calcite-silicate rocks share similarities with those in kimberlites and alkaline ultramafic rocks, exhibiting comparable profiles in REE, U, Th/U ratio, and other trace elements. In contrast, perovskites from the distinct skarns of the Akhmatov mine show divergent trace element contents, indicating a different origin.

The age data of the perovskites indicates endogenic activity in the South Urals Western Slope during the Cambrian period, challenging the skarn nature of this perovskite mineralization. The association of perovskite with magnesioferrite and forsterite, along with the absence of a clear spatial correlation between mineralized carbonate veins and the extent of gabbro metamorphism, suggests that the origin of the perovskite is unlikely to be due to low-temperature metamorphic processes. Overall, the evidence points to an origin akin to those found in carbonatites and kimberlites.

Author Contributions: Conceptualization, S.S.; methodology, E.L., E.S. and E.M.; validation, R.P. and A.K.; formal analysis, E.L., E.S. and E.M.; investigation, S.S.; resources, R.P.; data curation, R.P.; writing—original draft preparation, S.S.; writing—review and editing, A.K.; visualization, R.P.; supervision, L.S.; project administration, S.S.; funding acquisition, R.P. All authors have read and agreed to the published version of the manuscript.

Funding: This research was funded by the South Urals Federal Research Center of Mineralogy and Geoecology, grant number 122040600006-1 (FUUR-2022-0004).

Data Availability Statement: Data are contained within the article.

Acknowledgments: The authors are grateful for the constructive comments of the reviewers and editors, who greatly improved the quality of the manuscript.

Conflicts of Interest: The authors declare no conflicts of interest.

References

- Rose, G. Beschreibung einiger neuen Mineralien des Urals. *Ann. Der Phys. Und Chem.* **1839**, *48*, 551–573. [\[CrossRef\]](#)
- Mushketov, I.V. *Materials for the Study of the Geonostic Structure and Ore Resources of the Zlatoust Mining District in the Southern Urals*; Printing House of the Imperial Academy of Sciences: St. Petersburg, Russia, 1887; 231p. (In Russian)
- Pekov, I. *Minerals First Discovered on the Territory of the Former Soviet Union*; Ocean Pictures: Moscow, Russia, 1998; 369p.
- Popov, V.A.; Rassomakhin, M.A. Mineral assemblages of the Shishim mine in the Southern Urals. *Mineralogy* **2023**, *9*, 23–44. (In Russian) [\[CrossRef\]](#)
- Plat, G.G. Perovskite, loparite and Ba-Fe hollandite from the Schryburt Lake carbonatite complex, northwestern Ontario, Canada. *Mineral. Mag.* **1994**, *58*, 49–57. [\[CrossRef\]](#)
- Mitchell, R.H. *Perovskites: Modern and Ancient*; Almaz Press Inc.: Thunder Bay, ON, Canada, 2002; 316p.
- Batumike, J.M.; Griffin, W.L.; Belousova, E.A.; Pearson, N.J.; O'Reilly, S.Y.; Shee, S.R. LAM-ICP-MS U–Pb dating of kimberlitic perovskite: Eocene-Oligocene kimberlites from the Kundelungu Plateau, D.R. Congo. *Earth Planet. Sci. Lett.* **2008**, *267*, 609–619. [\[CrossRef\]](#)
- Wu, F.; Yang, Y.; Mitchell, R.H.; Li, Q.; Yang, J.; Zhang, Y. In situ U–Pb age determination and Nd isotopic analysis of perovskites from kimberlites in southern Africa and Somerset Island, Canada. *Lithos* **2010**, *115*, 205–222. [\[CrossRef\]](#)
- Chakhmouradian, A.R.; Reguir, E.P.; Kamenetsky, V.S.; Sharygin, V.V.; Golovin, A.V. Trace element partitioning in perovskite: Implications for the geochemistry of kimberlites and other mantle-derived under saturated. *Rocks Chem. Geol.* **2013**, *353*, 112–131. [\[CrossRef\]](#)
- Potter, N.J.; Ferguson, M.R.M.; Kamenetsky, V.S.; Chakhmouradian, A.R.; Sharygin, V.V.; Thompson, J.M.; Goemann, K. Textural evolution of perovskite in the Afrikanda alkaline-ultramafic complex, Kola Peninsula, Russia. *Contrib. Mineral. Petrol.* **2018**, *137*, 100. [\[CrossRef\]](#)
- Myasnikov, V.S. Mineral mines of the Shishim and Nazyam mountains. *Mineral. Ural.* **1954**, *1*, 250–268. (In Russian)
- Gekimyants, V.M. *Mineralogy of Titanium and Zirconium in Skarns, Rodingites, and Rodingite-Like Formations of the Western Urals*; MGU: Moscow, Russia, 2002; 20p. (In Russian)
- Belkovsky, A.I.; Loktina, I.N.; Nesterov, A.R. Mineral mines of the Shishimsky-Nazyamsky mountains: Pre-carbonatite skarns and early (oreless) carbonatites. *Probl. Petrog. Ore Form.* **1998**, 12–14. (In Russian)
- Popov, V.A. The Akhmatov Mine in the South Urals: Notes on Mineralogy. *Mineral. Alm.* **2012**, *17*, 8–46.
- Kholodnov, V.V.; Shagalov, E.S. The Upper and Lower Age Boundaries of the Middle Riphean (Ti-Fe-V) Intrusions of the Kusinsko-Kopanskaya Complex in the South Urals: U–Pb Dating of Zircons from the Medvedevskoe Deposit. *Dokl. Earth Sci.* **2012**, *446*, 1171–1175. [\[CrossRef\]](#)
- Kinny, P.D.; Griffin, B.J.; Heaman, L.M.; Brakhfogel, F.F.; Spetsius, Z.V. SHRIMP U–Pb Ages of Perovskite from Yakutian Kimberlites. *Russ. Geol. Geophys.* **1997**, *38*, 97–105.
- Ireland, T.R.; Compston, W.; Williams, I.S.; Wendt, I. U–Pb systematics of individual perovskite grains from the Allende and Murchison carbonaceous chondrites. *Earth Planet. Sci. Lett.* **1990**, *101*, 379–387. [\[CrossRef\]](#)
- Stepanov, S.Y.; Sharpenok, L.N.; Palamarchuk, R.S.; Glazov, A.I.; Palamarchuk, R.S. Distribution of trace elements in perovskite from skarns and calcite veins of the Chernaya rechka and Nazyam ridges (South Urals). *Mineralogy* **2017**, *3*, 61–70.
- Arakcheeva, A.V.; Lubman, G.U.; Pushcharovsky, D.Y.; Gekimyants, V.M.; Popov, V.A. Crystal structure and microtwinning of natural orthorhombic perovskite CaTiO₃. *Crystallogr. Rep.* **1997**, *42*, 46–54.
- Goldschmidt, V. *Atlas der Krystallformen*; University of Toronto: Toronto, ON, Canada, 1913. (In German)
- Stepanov, S.Y.; Puchkov, V.N.; Palamarchuk, R.S.; Popov, V.A.; Lepshina, E.N.; Sharpenok, L.N.; Antonov, A.V. The first evidence for Paleozoic endogenous activity on the Western slope of the Southern Urals. *Dokl. Earth Sci.* **2020**, *493*, 499–503. [\[CrossRef\]](#)
- Woolley, A.R. *Alkaline Rocks and Carbonatites of the World—Part 3: Africa*; The Geological Society: London, UK, 2001.
- Arzamastsev, A.; Arzamastseva, L.; Bea, F.; Montero, P. Rare earth elements in rocks and minerals from alkaline plutons of the Kola Peninsula, NW Russia, as indicators of alkaline magma evolution. *Russ. J. Earth Sci.* **2002**, *4*, 187–209. [\[CrossRef\]](#)

24. Alexandrov, S.M.; Troneva, M.A. Composition, mineral assemblages and genesis of serendibite-bearing magnesian skarns. *Geochem. Int.* **2006**, *44*, 665–680. [[CrossRef](#)]
25. Starikova, A.E.; Sklyarov, E.V.; Kotov, A.B.; Sal'nikova, E.B.; Fedorovskii, V.S.; Lavrenchuk, A.V.; Mazukabzov, A.M. Vein calciphyre and contact Mg skarn from the Tazheran massif (Western Baikal area, Russia): Age and genesis. *Dokl. Earth Science* **2014**, *457*, 1003–1007. [[CrossRef](#)]
26. Sklyarov, E.V.; Karmanov, N.S.; Lavrenchuk, A.V.; Starikova, A.E. Perovskites of the Tazheran Massif (Baikal, Russia). *Minerals* **2019**, *9*, 323. [[CrossRef](#)]
27. Chakhmouradian, A.R.; Mitchell, R.H. Compositional variation of perovskite group minerals from the carbonatite complexes of the Kola Alkaline Province, Russia. *Can. Mineral.* **1997**, *35*, 1293–1310.
28. Arzamastsev, A.; Arzamastseva, L. Paleozoic Tholeiite Magmatism in the Kola Province, Russia: Relations to Alkaline Magmatism. In Proceedings of the Goldschmidt, Prague, Czech Republic, 15–19 August 2011.
29. Mitchell, R.H. *Kimberlites, Orangeites and Related Rocks*; Plenum Press: New York, NY, USA, 1995; 410p.
30. Chakhmouradian, A.R.; Mitchell, R.H. Occurrence, alteration patterns and compositional variation of perovskite in kimberlites. *Can. Mineral.* **2000**, *38*, 975–994. [[CrossRef](#)]
31. Reguir, E.P.; Camacho, A.; Yang, P.; Chakhmouradian, A.R.; Kamenetsky, V.S.; Halden, N.M. Trace-element study and uranium–lead dating of perovskite from the Afrikanda plutonic complex, Kola Peninsula (Russia) using LA-ICP-MS. *Mineral. Petrol.* **2010**, *100*, 95–103. [[CrossRef](#)]
32. Chen, W.; Simonetti, A. Evidence for the Multi-Stage Petrogenetic History of the Oka Carbonatite Complex (Quebec, Canada) as Recorded by Perovskite and Apatite. *Minerals* **2014**, *4*, 437–476. [[CrossRef](#)]
33. Chalapathi Rao, N.V.; Fu-Yuan, R.H.; Li, Q.-L.; Lehmann, B. Mesoproterozoic U–Pb ages, trace element and Sr–Nd isotopic composition of perovskite from kimberlites of the Eastern Dharwar craton, southern India: Distinct mantle sources and a widespread 1.1 Ga tectonomagmatic event. *Chem. Geol.* **2013**, *353*, 48–64.
34. Ghobadi, M.; Gerdes, A.; Kogarko, L.; Hofer, H.; Brey, G. In situ LA-ICP-MS Isotopic and Geochronological Studies on Carbonatites and Phoscorites from the Guli Massif, Maymecha-Kotuy, Polar Siberia. *Geochem. Int.* **2018**, *56*, 766–783. [[CrossRef](#)]
35. Rass, I.T. Fractionation of microcomponents in coexisting high- and low-calcium alkaline-ultrabasic series of the Odikhincha massif (Polar Siberia). *Geochemistry* **2004**, *8*, 852–863. (In Russian)
36. Chernostrovets, A.N. The history of discovery and study of Zelentsov mineral mine (mine of the 3-rd magnetic bald peak) of the Nazyam mountains, Southern Urals. *Ural. Geol. J.* **2014**, *3*, 42–52. (In Russian)
37. Puchkov, V.N.; Kozlov, V.I.; Krasnobaev, A.A. Paleozoic U–Pb SHRIMP dating of magmatic rocks of the Bashkir megaanticlinorium. *Geol. Collect.* **2011**, *9*, 36–43. (In Russian)
38. Krasnobaev, A.A.; Puchkov, V.N.; Sergeeva, N.D. Polychronous zirconology of navysh volcanics of the Ai formation (Southern Urals). *Dokl. Earth Sci.* **2018**, *478*, 56–61. [[CrossRef](#)]

Disclaimer/Publisher's Note: The statements, opinions and data contained in all publications are solely those of the individual author(s) and contributor(s) and not of MDPI and/or the editor(s). MDPI and/or the editor(s) disclaim responsibility for any injury to people or property resulting from any ideas, methods, instructions or products referred to in the content.